mater.scichina.com link.springer.com

Published online 3 June 2020 | https://doi.org/10.1007/s40843-020-1344-x
*Sci China Mater* 2020, 63(9): 1750–1758

# High-pressure synthesis, crystal structure and physical properties of a new Cr-based arsenide $La_3CrAs_5$

Lei Duan[1,2], Xiancheng Wang[1*], Fangyang Zhan[3], Jun Zhang[1,2], Zhiwei Hu[4], Jianfa Zhao[1,2], Wenmin Li[1,2], Lipeng Cao[1,2], Zheng Deng[1], Runze Yu[1], Hong-Ji. Lin[5], Chien-Te. Chen[5], Rui Wang[3*] and Changqing Jin[1,2,6*]

**ABSTRACT** **In La-Cr-As system, the first ternary compound $La_3CrAs_5$ has been successfully synthesized under high-pressure and high-temperature conditions. $La_3CrAs_5$ crystallizes into a hexagonal $Hf_5Sn_3Cu$-anti type structure with a space group of $P6_3/mcm$ (No. 193) and lattice parameters of $a=b=8.9845$ Å and $c=5.8897$ Å. The structure contains face-sharing octahedral $CrAs_6$ chains along the *c*-axis, which are arranged triangularly in the *ab*-plane and separated by a significantly large distance of 8.9845 Å. The magnetic properties, resistivity and specific heat measurements were performed. $La_3CrAs_5$ exhibits a metallic state with Fermi liquid behavior at low temperatures and undergoes a ferromagnetic transition at Curie temperature $T_C$ ~50 K. First-principles theoretical studies were conducted to calculate its band structure and density of states (DOS), which indicated that the non-negligible contribution of La to the DOS near the Fermi level caused $La_3CrAs_5$ to be a three-dimensional (3D) metal. The crystal orbital Hamilton population (–COHP) was also calculated to explain the global stability and bonding characteristics in the structure of $La_3CrAs_5$.**

**Keywords:** Cr-based arsenide, ferromagnetic metal, high pressure synthesis, spin chain

## INTRODUCTION

The chrome arsenide related compounds have attracted much attention due to their various structures and rich physical properties, such as unconventional superconductivity (SC) [1–7]. The binary compound CrAs with noncollinear antiferromagnetic ground state, which adopts an orthorhombic MnP-type structure, was reported to exhibit SC at 2 K by suppressing the antiferromagnetic order *via* the application of external high pressures above 0.8 GPa [7,8]. In addition, the recent discovered quasi-one-dimensional Cr-based compounds $A_2Cr_3As_3$ (A=Na, K, Rb, Cs) were found to be superconducting at ambient pressure with the maximum superconducting transition temperature $T_s$ ~8.6 K [4]. These $A_2Cr_3As_3$ compounds crystallize in a hexagonal crystal lattice, which consists of infinite $[(Cr_3As_3)^{2-}]_\infty$ double-walled linear sub-nanotubes separated by the alkali-metal cations. When the ionic diameter of alkaline earth metals increases from $Na^+$ ions to $Cs^+$ ions, the superconducting $T_s$ monotonously decreases from 8.6 to 2.2 K [1,4–6]. The theory predicted that these quasi 1D Cr-based compounds are close to a novel in-out co-planar magnetic ground state and the SC is related to the magnetism [9]. It is interesting that *via* removing an $A^+$ ion per formula from $A_2Cr_3As_3$, another type quasi-1D compounds $ACr_3As_3$ with similar crystal structure can be prepared [2,3,10]. The single-crystalline samples of $ACr_3As_3$ (A=K and Rb) exhibit a superconducting phase transition at $T_s$=5.0 and 7.3 K, respectively [2,3].

Besides the above superconducting Cr-based compounds, the ternary Cr-based compounds $AmCr_2As_2$ (Am=Sr, Ba, Eu) with tetragonal $ThCr_2Si_2$-type tetragonal

[1] Beijing National Laboratory for Condensed Matter Physics, Institute of Physics, Chinese Academy of Sciences, Beijing 100190
[2] School of Physics, University of Chinese Academy of Sciences, Beijing 100190
[3] Institute for Structure and Function & Department of Physics, Chongqing University, Chongqing 400044
[4] Max Plank Institute for Chemical Physics of Solids, Dresden D-01187
[5] National Synchrotron Radiation Research Center, Hsinchu 30076
[6] Materials Research Lab at Songshan Lake, Dongguan 523808
[*] Corresponding authors (emails: wangxiancheng@iphy.ac.cn (Wang X); rcwang@cqu.edu.cn (Wang R); jin@iphy.ac.cn (Jin C))

  

structure display rich magnetic properties [11–13]. These compounds contain alternate CrAs layers, which consist of edge-sharing $CrAs_4$ tetrahedra, and Am layers stacked along the *c* axis. $SrCr_2As_2$ and $BaCr_2As_2$ undergo an itinerant *G*-typed anti-ferromagnetic (AFM) ground state with high Néel temperatures (590 and 580 K, respectively) [11,13], while $EuCr_2As_2$ displays more complex magnetism owing to competing FM and AFM interactions with a large negative magnetoresistance (~−24%) [12].

The ternary Cr-based arsenides containing alkali or alkaline-earth cations have been studied extensively. However, no information is available for ternary Cr-based arsenides containing $La^{3+}$ cations to our knowledge. Pressure is another key parameter to contribute increasingly to innovations in materials sciences beyond temperature and composition. High pressure is capable to generate plenty of new materials or new phases, which can hardly be synthesized under ambient pressure [14]. We set out to conduct an exploratory study on the La-Cr-As system using the high pressure technique and discovered a new ternary arsenide $La_3CrAs_5$. In this work, we report on the synthesis, crystal and electronic structures, chemical bonding and physical properties of $La_3CrAs_5$. Our results indicate that the title compound presents a three-dimensional (3D) metallic behavior with a ferromagnetic transition at ~50 K.

## EXPERIMENTAL SECTION

Polycrystalline sample of $La_3CrAs_5$ was synthesized under the conditions of high-pressure and high-temperature. Commercially available lumps of La (Alfa, >99.99% pure), lumps of As (Alfa, >99.999% pure), and Cr powder (Alfa, >99.99% pure) were used as the starting materials. The precursor LaAs was prepared by the reaction of the La and As lumps in an alumina crucible sealed in an evacuated quartz tube at 700°C for 24 h. The obtained LaAs, Cr and As were homogenously mixed at the molar ratio of 3:1:2, pressed into a pellet with a diameter of 6 mm, and then subjected to high-pressure synthesis under 5.5 GPa pressure and 1400°C for 40 min in a cubic-anvil-type high-pressure apparatus, of which the details had been reported in Refs. [15,16].

Room-temperature powder X-ray diffraction (PXRD) was conducted on a Rigaku Ultima VI (3 kW) diffractometer using Cu Kα radiation ($\lambda$=1.54060 Å) generated at 40 kV and 40 mA. The XRD data were collected with a scanning rate of 1° $min^{-1}$ and a scanning step length of 0.02°. Rietveld refinements on the diffraction patterns were performed using GSAS software packages. Magnetic measurements were performed using a superconducting quantum interference device (SQUID). The temperature dependence of the magnetic susceptibility measurement was carried out in the temperature range of 2–300 K with the field of 0.1 T. Isothermal dependences of magnetization were measured at 2 and 100 K with the magnetic field varying from 0 to 7 T. The electrical resistance in the 2–300 K temperature range was measured using the standard four-probe method in a physical property measuring system (PPMS). Specific heat measurement was carried out using PPMS from 2 to 100 K. Soft X-ray absorption spectroscopy (XAS) at the Cr $L_{2,3}$-edges of $La_3CrAs_5$ was studied at the beamline BL11A of the NSRRC in Taiwan, China using total electron yield mode.

Electronic structure calculations and bonding analyses on $La_3CrAs_5$ were carried out in the framework of the density functional theory (DFT) [17] encoded in the Vienna *Ab initio* Simulation Package (VASP) [18]. The core-valence electron interactions were described by the projector augmented-wave method [19]. A plane-wave cutoff energy was set to 500 eV. We chose the exchange-correlation functional as the generalized gradient approximation (GGA) with the Perdew-Burke-Ernzerhof formalism [20]. The full Brillouin zone (BZ) was sampled by a 8×8×12 Monkhorst-Pack mesh-grid [21]. Due to the correlation effects of d electrons in Cr and La atoms, we employed GGA+*U* scheme [22]. The on-site repulsions were chosen to *U*=2.5 eV for Cr 3d orbitals [23] and *U*=5 eV for La 5d orbitals [24]. It is also found that the similar electronic features have been confirmed in a large range of *U* 1.5–5.0 eV for Cr and 2.0–8.0 eV for La.

## RESULTS AND DISCUSSION

Fig. 1 shows the Rietveld refinement of room temperature PXRD pattern of $La_3CrAs_5$. All the peaks can be indexed using a hexagonal structure with the lattice parameters of *a*=*b*=8.9845 Å and *c*=5.8897 Å. Here, the structure of $La_3TiSb_5$ with the space group of $P6_3/mcm$ (No. 193) [25], was adopted as the initial model to carry out the refinement for the XRD data. The refinement smoothly converges to $\chi^2$=2.9, $R_p$=2.5% and $R_{wp}$=4.9%. The crystallographic data were obtained and summarized as shown in Table 1. Selected important bond distances and angles are demonstrated in Table 2.

The sketch of the crystal structure of $La_3CrAs_5$ is presented in Fig. 2a, viewed with the projection along the [001] direction. The crystal structure consists of face-sharing octahedral $CrAs_6$ chains along the *c*-axis, which are arranged triangularly in the *ab*-plane. Fig. 2b shows

  

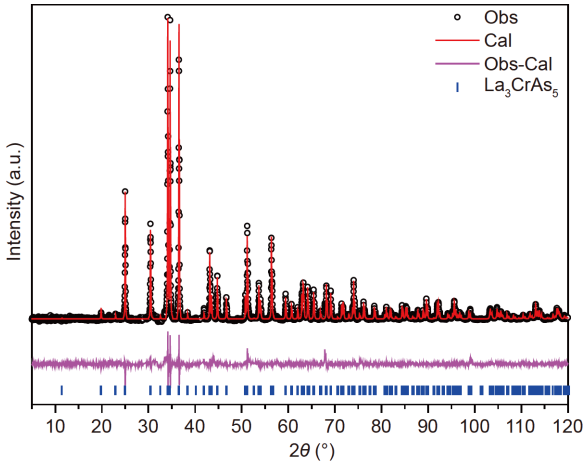


**Figure 1** The PXRD pattern of $La_3CrAs_5$ and the refinement with the space group of $P6_3/mcm$ (No. 193).

**Table 1** The summary of the crystallographic data at room temperature for $La_3CrAs_5$[a]

| Site | Wyck. | *x* | *y* | *z* | *U* (Å) |
|---|---|---|---|---|---|
| La | 6g | 0.6227(7) | 0 | 1/4 | 0.0122 |
| Cr | 2b | 0 | 0 | 0 | 0.0239 |
| As1 | 6g | 0.2417(8) | 0 | 1/4 | 0.0173 |
| As2 | 4d | 1/3 | 2/3 | 0 | 0.0285 |

a) Space group: $P6_3/mcm$—hexagonal (No.193); $a$=8.9845(1) Å, $c$=5.8897(1) Å; $V$=411.73(1) Å$^3$; $\chi^2$=2.9, $R_p$=2.5%, $R_{wp}$=4.9%.

**Table 2** Selected distances between adjacent atoms and angles

| Selected atom | Distance (Å) and angle (°) | Selected atom | Distance (Å) and angle (°) |
|---|---|---|---|
| La–As1(×2) | 3.1864(1) | La–La | 3.6795(7) |
| La–As2(×4) | 3.1799(1) | As2–As2[a] | 5.1873(0) |
| La–As1(×2) | 2.9738(5) | Cr–As1 | 2.6243(1) |
| Cr–Cr (×2)[a] | 2.9448(1) | As1–Cr–As1 | 88.408(5) |
| Cr–Cr[b] | 8.9845(1) | | 91.592(6) |

a) The intrachain distance; b) the interchain distance.

the details of octahedral $CrAs_6$ chains. The As1 anions located on the site of ($x$, 0, 1/4) surround the center ions of Cr to form $CrAs_6$ octahedron. In the $CrAs_6$ octahedron, all the distances between Cr and As1 are 2.6243(1) Å, which is comparable to that in binary CrAs (2.45–2.57 Å) [8]. The bond angles of As1–Cr–As1 are 88.408° and 91.592°, which deviate from the value of 90° in a regular octahedron and indicate that the $CrAs_6$ octahedron is slightly compressed along the $c$ axis. Within octahedral $CrAs_6$ chains, the distance between the corresponding Cr ions in the chain (2.9448 Å) is longer than the metallic bond length of Cr (~2.5 Å) [26], and it is not obvious if metal-metal bonding is operative. Since the electrostatic repulsion between the cationic centers of adjacent octahedra would rather lead to elongation of the octahedron along the stacking direction, a bonding interaction between the Cr atoms must be present in $La_3CrAs_5$. Our first-principles calculations (*vide infra*) show that despite the relatively long distance between corresponding Cr ions, the Cr ions display significant bonding interactions, which may explain the observed distortion of the $CrAs_6$ octahedron.

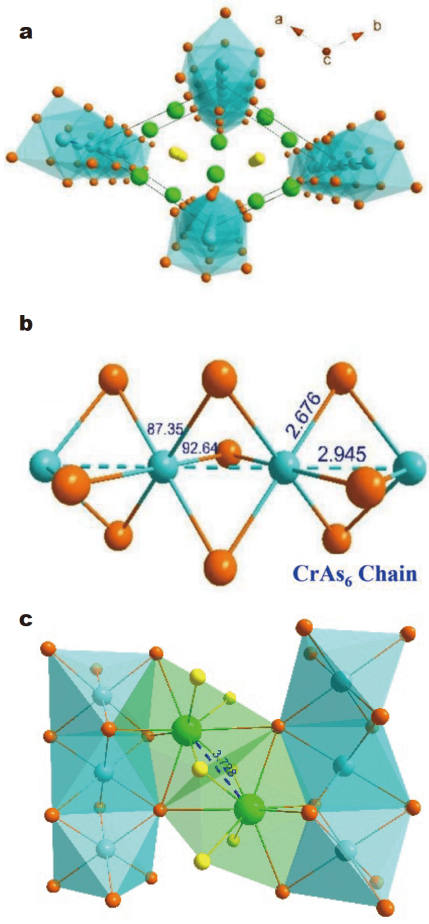


**Figure 2** (a) The crystal structure of $La_3CrAs_5$ with the projection along the $c$ axis, showing the triangular lattice form and chain structure characteristic. (b) The sketch of $CrAs_6$ octahedron chain in $La_3CrAs_5$. (c) The partial structure of $La_3CrAs_5$, displaying the bridge of $LaAs_9$ polyhedron between $CrAs_6$ octahedral chains and As2 chains.

Besides the $CrAs_6$ chains, the anions As2 located at the center of the triangular lattice with the site of (1/3, 2/3, 0) are space-equally aligned along the $c$ axis to form the As-chains. In the As-chains, the distance of the corre-

  

sponding As2 (2.9448 Å) is obviously larger than the typical bond length of As–As (~2.5 Å) [27]. The moderate distance of As2–As2 hints the 4p-orbitals of As2 in the linear As-chains can be overlapped, and thus, As2 ions should be a hypervalent oxidation state. Similar hypervalent Bi ions in Bi-chain of $La_3TiBi_5$ compound have been reported [28]. These octahedral $CrAs_6$ chains and As-chains are separated by La ions. The distance between the $CrAs_6$ chains is 8.9845 Å, which is significantly larger than that between adjacent Cr ions in the chain. Thus, the crystal structure of $La_3CrAs_5$ exhibits 1D spin chain characteristic.

Fig. 2c shows the partial structure of $La_3CrAs_5$, displaying the connection of $CrAs_6$ chains by face-sharing $LaAs_9$ polyhedrons. There are nine As-ligands surrounding the center La ions, of which four As1 ligands come from the same $CrAs_6$ chain, one As1 ligand from the other $CrAs_6$ chain and the other four As2 ligands from the As2 chains. The distances of La–As range from 2.9738–3.1864 Å, which is comparable to the binary arsenides of LaAs (~3.08 Å) and $LaAs_2$ (3.12–3.25 Å) [29]. In addition, it is noted that the distance of the corresponding La ions is 3.6795 Å, which is comparable to the interatomic distance of La (~3.65 Å) [30].

The electronic band structure and spin-resolved partial density of states (DOS) for $La_3CrAs_5$ were calculated as shown in Fig. 3. The total energy calculations with different magnetic configurations suggest that $La_3CrAs_5$ is a ferromagnetic metal with the paralleled magnetic moments of two Cr atoms in a unit cell. The 4s and 3d occupation numbers of Cr atoms are 0.25 and 4.07, respectively. The calculated effective magnetic moment is 3.2 $\mu_B$/Cr, which is in good agreement with the following measurement results. The results indicate a coexistence of localized and itinerant electrons in $La_3CrAs_5$. In the band structure, there are several bands crossing the Fermi level along the $c^*$ axis including the $\Gamma$-$A$ path, $H$-$K$ path, and $M$-$L$ path, which suggests it is conducting along the chain direction. In addition, along the $A$-$H$, $K$-$\Gamma$ and $\Gamma$-$M$ paths, which are perpendicular to the $c^*$ axis, there are several bands cutting the Fermi level as well. As a result, the electrons in $La_3CrAs_5$ can hop coherently between each two of the conducting chains. From the partial DOS of $La_3CrAs_5$, it can be seen that the primary contribution to the conduction band is from Cr and As atoms. In addition, the contribution of La 5d-orbital to the DOS near the Fermi level cannot be negligible although it is much less than those of As and Cr. It is suggested that the $La^{3+}$ ions are not perfectly ionic and bridge the conducting chains to cause the 3D metallic behavior.

To understand the bonding features of $La_3CrAs_5$, we further calculated the crystal orbital Hamilton population (COHP) as implemented in the LOBSTER code [31], as shown in Fig. 4. The optimized bond distances and the absolute integral values of −ICOHP are listed in Table 3. The results show that the primary bonding interactions come from the Cr–As and La–As. The individual heteroatomic La–As orbital interactions have −ICOHP values of 1.74 and 1.53 eV for La–As1 and La–As2, respectively. These Cr–As1 interactions are strongly bonding (with an integrated −COHP of 1.42 eV per bond) with all bonding states below the Fermi level and antibonding ones above the Fermi level. The Cr–Cr within the face-sharing octahedral chains contacts also show predominantly bonding interactions (−ICOHP of 0.82 eV per bond), resulting in a large contribution to the

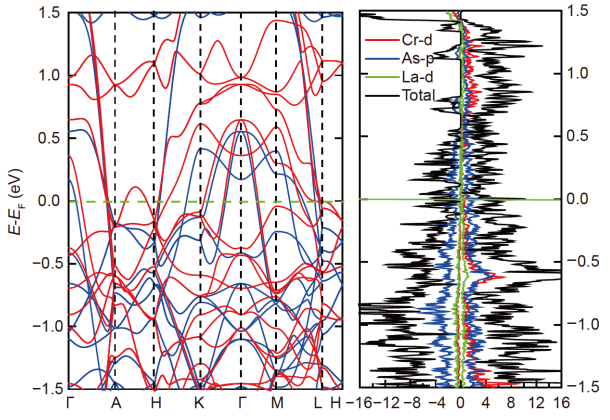


**Figure 3** The calculated electronic band structures along high symmetry paths where the spin up and spin down bands are denoted by red and blue lines (right panel) and the spin-resolved partial density of states (left panel).

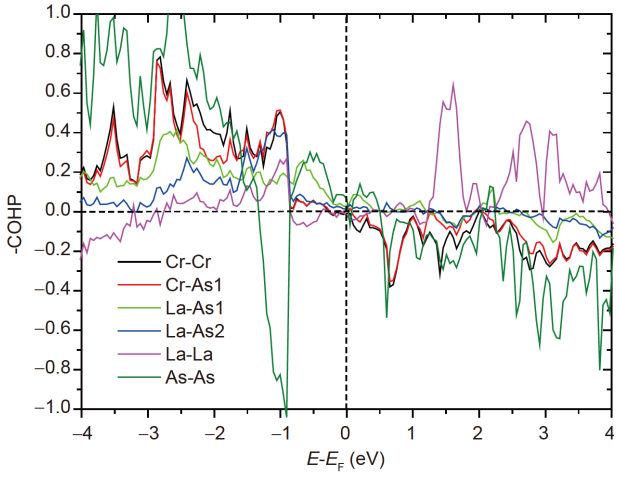


**Figure 4** −COHP plot for the selected interactions.

  

**Table 3** Selected interactions, their distances after structure relaxation and their corresponding ICOHPs per bond in $La_3CrAs_5$

| Interaction | Distance (Å) | ICOHP per bond (eV) |
|---|---|---|
| Cr–Cr | 2.986 | −0.82 |
| Cr–As1 | 2.616 | −1.42 |
| La–As1 | 2.998 | −1.74 |
| La–As2 | 3.215 | −1.53 |
| As2–As2 | 2.986 | −1.58 |
| La–La | 3.804 | −0.96 |

global stability. The equally long As2–As2 interactions within the linear chains show both bonding and antibonding character below the Fermi energy ($E_F$) with strong bonding (−ICOHP of 1.53 eV per bond). Such a bonding picture appears to be typical for hypervalent interactions in metal pnictides. Furthermore, the −ICOHP value of La–La orbital interactions is 0.96 eV. This indicates a weak La–La interaction in $La_3CrAs_5$ which is likely one of the reasons for the attendance of the 3D electronic structure in this compound.

It is well known that soft XAS at the 3d transition-metal $L_{2,3}$ edges is very sensitive to the electronic structure and the local environment of the 3d ions, and thus it becomes standard tool to study the charge state of 3d transition-metal elements in the new materials [32–34]. The Cr-$L_{2,3}$ spectra of $La_3CrAs_5$ together with that of $Cr_2O_3$ as a $Cr^{3+}$ reference is shown in Fig. 5. Compared with sharpness of the multiplet features of the main peak for the Cr-$L_{2,3}$ edge of $Cr_2O_3$, the Cr-$L_{2,3}$ spectrum of $La_3CrAs_5$ is very broad, indicating the strongly delocalized nature for the 3d states in the metallic $La_3CrAs_5$. The Cr-$L_{2,3}$ spectra of $La_3CrAs_5$ is shifted by more than 1 eV to lower energies with respect to the spectrum of $Cr_2O_3$. This can be interpreted as a relative low valence state, since the ground

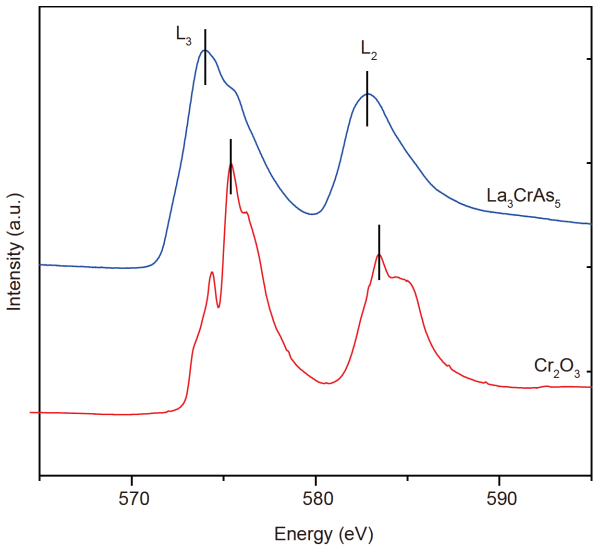


**Figure 5** Cr-$L_{2,3}$ XAS of $La_3CrAs_5$ with that of $Cr_2O_3$ as $Cr^{3+}$ reference.

state of metal has a non-integer filling of 3d shell and $E_f$ level locates within broad 3d band. In fact, 3d occupation number of ~4.08 per Cr ion was obtained from our above band structure calculation.

Fig. 6a displays the temperature dependence of magnetic susceptibility $\chi(T)$ and inverse magnetization $\chi^{-1}(T)$ for $La_3CrAs_5$ measured with $H$=1000 Oe. The magnetic susceptibility increases sharply at ~50 K, exhibiting a ferromagnetic transition. The temperature derivative of magnetic susceptibility is also presented (shown in the inset of Fig. 6a). The peak corresponding to the ferromagnetic transition can be clearly observed and $T_C$ is determined to be 50 K. The field-cooling (FC) and zero-field-cooling (ZFC) curves are overlapped in the whole temperature range, which suggests that the coercive force is less than 1000 Oe. The temperature range of 150 to

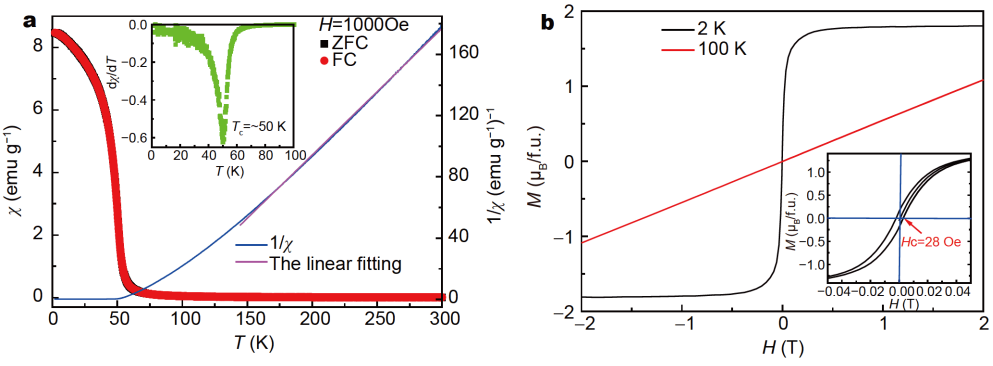


**Figure 6** (a) Temperature dependence of magnetic susceptibility $\chi(T)$ (left axis) and inverse magnetization $\chi^{-1}(T)$ (right axis) for $La_3CrAs_5$. The purple line is the fit of Curie-Weiss law between 150 and 300 K. The inset shows d$\chi$/d$T$ *vs.* $T$. (b) The magnetic hysteresis curve measured at 2 and 100 K. The inset presents the enlarged view of the low-field data at 2 K.

300 K was selected for fitting the high-temperature susceptibility with Curie-Wiess law $1/\chi=(T-T_\theta)/C$, also shown in Fig. 6a, where $C$ is the Curie constant and $T_\theta$ is the Weiss temperature. After the fitting, the Weiss temperature $T_\theta$ and effective moment $\mu_{eff}$ can be obtained. The value of $T_\theta$ is about 86.1 K, much higher than $T_C$, which suggests that the intrachain spin correlations have been developed far above $T_C$. The positive value of $T_\theta$ indicates the predominant interaction is ferromagnetic. The estimated $\mu_{eff}$ is 3.11 $\mu_B$/Cr, which is even smaller than the spin-only value of 3.87 $\mu_B$/Cr for $Cr^{3+}$ ion with $S$=3/2. Furthermore, the Cr-$L_{2,3}$ spectra of $La_3CrAs_5$ reveals that the valence state of Cr is much lower than +3, which indicates partial electrons in 3d orbital of Cr are itinerant. The ferromagnetic nature was confirmed by isothermal magnetization measured at 2 and 100 K as shown in Fig. 6b. The magnetization at 100 K is linearly dependent on the magnetic field, displaying a paramagnetic behavior. For the $M$-$H$ curve at 2 K, the magnetization is saturated at low magnetic field with the coercive force ~30 Oe, as shown in the inset of Fig. 6b. The saturation magnetization $\mu_s$ is about 1.8 $\mu_B$ and significantly smaller than the expected for a localized spin-only moment for high-spin $Cr^{3+}$ ion. Given the values of $\mu_{eff}$ and $\mu_s$, the Rhodes-Wolfarth ratio (RWR) can be calculated. According to Rhodes-Wolfarth, RWR can be defined as $\mu_c/\mu_s$, where $\mu_c$ is related to the number of moving carriers and can be obtained from the relation of $\mu^2_{eff}=\mu_c(\mu_c+2)$. For a localized system, the value of RWR should be 1, or the system diverges for itinerant ferromagnets [35,36]. In our case, the obtained RWR=1.26 indicates the existence of itinerant ferromagnetism in $La_3CrAs_5$.

Fig. 7a displays the resistivity $\rho(T)$ of $La_3CrAs_5$ measured within the temperature range from 2 to 300 K, which exhibits a metallic behavior with the room-temperature resistivity $\rho$ ~2.2 μΩ cm (300 K).

There is an anomaly at about 50 K, where the slope of resistivity decreases rapidly, corresponding to the ferromagnetic transition seen in the susceptibility data. To clearly display the anomaly, we plotted the temperature derivative of resistivity, as shown in the left inset of Fig. 7a, where a peak is observed at $T_C$. Generally, the resistivity should have a sudden fall corresponding to ferromagnetic transition since the electron scattering should be reduced due to the spin ferromagnetic ordering. For example, ferromagnetic quasi two-dimensional compounds $Fe_3GeTe_2$ undergoes a ferromagnetic transition at 220 K, and the resistivity drops sharply corresponding to the spin ordering [37]. The right inset of Fig. 7a shows the enlarged resistivity at low temperature. The low-temperature resistivity can be well fitted by the formula of $\rho=\rho_0+AT^2$, where $\rho_0$ and $A$ represent the residual resistivity and $T^2$-term coefficient, respectively. The values of parameters $\rho_0$=0.40 μΩ cm and $A$=$1.27\times10^{-4}$ μΩ cm $K^{-2}$ are obtained. Thus, the metallic $La_3CrAs_5$ at low temperature follows the Fermi liquid behavior.

The specific heat (SH) $C_p(T)$ curve between 2 and 100 K for $La_3CrAs_5$ is shown in Fig. 7b. Apparently, a small anomaly is observed near $T_C$ ~50 K, which confirms that there happens a long-range magnetic ordering transition. The small kink is a common feature for a quasi 1D spin chain system, where most of the magnetic entropy has

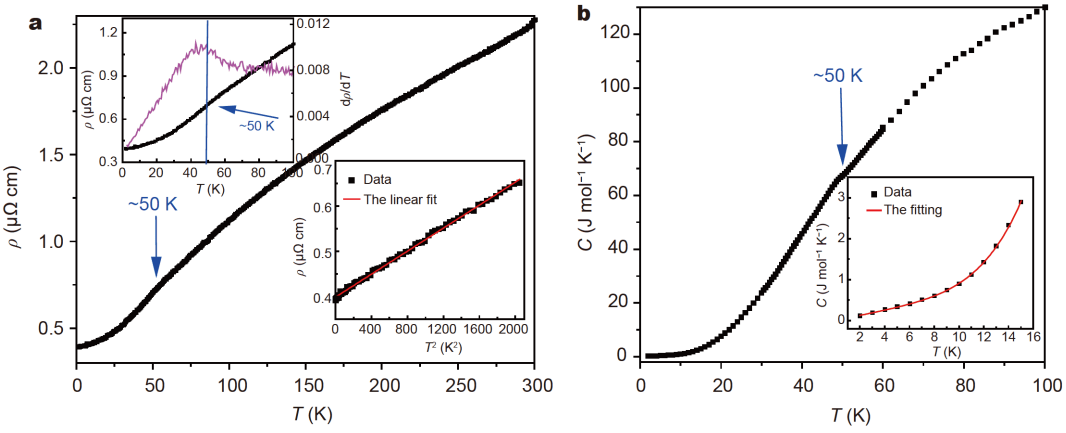


**Figure 7** (a) Temperature dependence of resistivity of $La_3CrAs_5$. The left inset shows the temperature dependence of d$\rho$/d$T$; The right inset shows the $T^2$ variation of $\rho$ at low temperature (2–45 K). (b) Temperature-dependent heat capacity between 2 and 100 K for $La_3CrAs_5$. The inset displays the fitting results of heat capacity at low temperature.

  

been released far above the ordering transition temperature since the short-range spin correlation has been developed gradually [38–41]. The inset of Fig. 7b shows the enlarged view of $C_p(T)$ below 15 K. The low-temperature $C_p(T)$ was fitted by the equation of $C_p(T)=\gamma T+[\beta T^3+\sigma T^5]$, where the two terms respect the contributions of the electronic SH and phonon SH, respectively. The fitted values are $\gamma$=62.3 mJ mol$^{-1}$ K$^{-2}$, $\beta$=0.0449 mJ mol$^{-1}$ K$^{-4}$ and $\sigma$=0.00239 mJ mol$^{-1}$ K$^{-6}$. The Debye temperature $\Theta_D$ of $La_3CrAs_5$ can be derived from the value of parameter $\beta$ to be 157.3 K by the formula of $\Theta_D=(12\pi^4Rn/5\beta)^{1/3}$, where $n$=9 is the number of atoms in the unit cell.

Since $La_3CrAs_5$ consists of $CrAs_6$ chains, we can have a comparison of its properties with similar compounds with 1D spin chains. $Ba_9V_3Se_{15}$ is such a typical example, which consists of octahedral $VSe_6$ chains. Similar to $La_3CrAs_5$, the spin chains in $Ba_9V_3Se_{15}$ are separated with a large distance of 9.57 Å [41]. In quasi 1D spin chain system, the interchain coupling governs the long-range order although it generally is significantly smaller than intrachain coupling. For $Ba_9V_3Se_{15}$, because of the large interchain distance and the semiconducting nature, the interchain coupling is very small and leads to a very low ferrimagnetic transition temperature about 2.5 K [41]. However, in contrast to $Ba_9V_3Se_{15}$, $La_3CrAs_5$ is a 3D metal and undergoes a long-range order at a relative high temperature of 50 K. Therefore, it is suggested that the interchain coupling in $La_3CrAs_5$ should be much larger than that of $Ba_9V_3Se_{15}$, owing to the existence of itinerant electrons, and thus gives rise to long-range ferromagnetic order at higher temperature.

## CONCLUSIONS

A new compound, $La_3CrAs_5$, which is the first ternary phase in the La-Cr-As system, was synthesized under high pressure and high temperature conditions. The chemical features, and physical properties of $La_3CrAs_5$ were also explored. The compound crystallizes into a hexagonal $Hf_5Sn_3Cu$-anti type structure, which contains face-sharing octahedral $CrAs_6$ chains and these spin chains are separated by a large distance of 8.9838 Å. The physical measurements reveal a metallic state with Fermi liquid behavior at low temperature, accompanying a ferromagnetic transition at $T_C$ ~50 K. Electronic structure calculations indicate that the contribution of La to the DOS near the Fermi level is non-negligible, which makes this compound to be a 3D metal. It is speculated that the interchain coupling should be mediated *via* the itinerant electrons, which plays an important role in the formation of the long-range magnetic order. The mechanism of magnetism in $La_3CrAs_5$ needs further work to study.

**Received 14 January 2020; accepted 11 April 2020; published online 3 June 2020**


1 Bao JK, Liu JY, Ma CW, *et al.* Superconductivity in quasi-one-dimensional $K_2Cr_3As_3$ with significant electron correlations. Phys Rev X, 2015, 5: 011013
2 Liu T, Mu QG, Pan BJ, *et al.* Superconductivity at 7.3 K in the 133-type Cr-based $RbCr_3As_3$ single crystals. Euro Phys Lett, 2017, 120: 27006
3 Mu QG, Ruan BB, Pan BJ, *et al.* Superconductivity at 5 K in quasi-one-dimensional Cr-based $KCr_3As_3$ single crystals. Phys Rev B, 2017, 96: 140504
4 Mu QG, Ruan BB, Pan BJ, *et al.* Ion-exchange synthesis and superconductivity at 8.6 K of $Na_2Cr_3As_3$ with quasi-one-dimensional crystal structure. Phys Rev Mater, 2018, 2: 034803
5 Tang ZT, Bao JK, Liu Y, *et al.* Unconventional superconductivity in quasi-one-dimensional $Rb_2Cr_3As_3$. Phys Rev B, 2015, 91: 020506
6 Tang ZT, Bao JK, Wang Z, *et al.* Superconductivity in quasi-one-dimensional $Cs_2Cr_3As_3$ with large interchain distance. Sci China Mater, 2015, 58: 16–20
7 Wu W, Cheng J, Matsubayashi K, *et al.* Superconductivity in the vicinity of antiferromagnetic order in CrAs. Nat Commun, 2014, 5: 5508
8 Selte K, Kjekshus A, Jamison WE, *et al.* Magnetic structure and properties of CrAs. Acta Chem Scand, 1971, 25: 1703–1714
9 Wu XX, Le CC, Yuan J, *et al.* Magnetism in quasi-one-dimensional $A_2Cr_3As_3$ (A=K, Rb) superconductors. Chin Phys Lett, 2015, 32: 057401
10 Tang ZT, Bao JK, Liu Y, *et al.* Synthesis, crystal structure and physical properties of quasi-one-dimensional $ACr_3As_3$ (A=Rb, Cs). Sci China Mater, 2015, 58: 543–549
11 Das P, Sangeetha NS, Lindemann GR, *et al.* Itinerant G-type antiferromagnetic order in $SrCr_2As_2$. Phys Rev B, 2017, 96: 014411
12 Paramanik UB, Prasad R, Geibel C, *et al.* Itinerant and local-moment magnetism in $EuCr_2As_2$ single crystals. Phys Rev B, 2014, 89: 144423
13 Singh DJ, Sefat AS, McGuire MA, *et al.* Itinerant antiferromagnetism in $BaCr_2As_2$: experimental characterization and electronic structure calculations. Phys Rev B, 2009, 79: 094429
14 Jin CQ. Using pressure effects to create new emergent materials by design. MRS Adv, 2017, 2: 2587–2596
15 Jin CQ, Adachi S, Wu XJ, *et al.* 117 K superconductivity in the Ba-Ca-Cu-O system. Physica C, 1994, 223: 238–242
16 Jin CQ, Wu XJ, Laffez P, *et al.* Superconductivity at 80 K in $(Sr,Ca)_3Cu_2O_{4+\delta}Cl_{2-y}$ induced by apical oxygen doping. Nature, 1995, 375: 301–303
17 Kohn W, Sham LJ. Self-consistent equations including exchange and correlation effects. Phys Rev, 1965, 140: A1133–A1138
18 Kresse G, Furthmüller J. Efficient iterative schemes for *ab initio* total-energy calculations using a plane-wave basis set. Phys Rev B, 1996, 54: 11169–11186
19 Kresse G, Joubert D. From ultrasoft pseudopotentials to the projector augmented-wave method. Phys Rev B, 1998, 59: 1758–1775
20 Perdew JP, Burke K, Ernzerhof M. Generalized gradient approximation made simple. Phys Rev Lett, 1996, 77: 3865–3868
21 Monkhorst HJ, Pack JD. Special points for brillouin-zone integrations. Phys Rev B, 1976, 13: 5188–5192


  

22 Liechtenstein AI, Anisimov VI, Zaanen J. Density-functional theory and strong interactions: orbital ordering in Mott-Hubbard insulators. Phys Rev B, 1995, 52: R5467–R5470
23 Bisti F, Rogalev V , Karolak M, *et al.* Weakly-correlated nature of ferromagnetism in nonsymmorphic $CrO_2$ revealed by bulk-sensitive soft-X-ray ARPES. Phys Rev X, 2017, 7: 041067
24 Wu M. High-temperature intrinsic quantum anomalous Hall effect in rare earth monohalide. 2D Mater, 2017, 4: 021014
25 Bollore G, Ferguson MJ, Hushagen RW, *et al.* New ternary rare-earth transition-metal antimonides $RE_3MSb_5$ (RE=La, Ce, Pr, Nd, Sm; M=Ti, Zr, Hf, Nb). Chem Mater, 1995, 7: 2229–2231
26 Kjekshus A, Skaug KE, Sæthre LJ, *et al.* On the phases $Cr_2As$, $Fe_2As$, $Co_2As$, and $Rh_2As$. Acta Chem Scand, 1972, 26: 2554–2556
27 Feng W, Cui S, Hu H, *et al.* First-principles study of A7 to simple cubic phase transformation in As. Physica B-Condensed Matter, 2007, 400: 22–25
28 Murakami T, Yamamoto T, Takeiri F, *et al.* Hypervalent bismuthides $La_3MBi_5$ (M=Ti, Zr, Hf) and related antimonides: absence of superconductivity. Inorg Chem, 2017, 56: 5041–5045
29 Murray JJ, Taylor JB. Halide vapor transport of binary rare-earth arsenides, antimonides and tellurides. J Less Common Met, 1970, 21: 159–167
30 Piermarini GJ, Weir CE. Allotropy in some rare-earth metals at high pressures. Science, 1964, 144: 69–71
31 Maintz S, Deringer VL, Tchougréeff AL, *et al.* LOBSTER: a tool to extract chemical bonding from plane-wave based DFT. J Comput Chem, 2016, 37: 1030–1035
32 Hollmann N, Hu Z, Willers T, *et al.* Local symmetry and magnetic anisotropy in multiferroic $MnWO_4$ and antiferromagnetic $CoWO_4$ studied by soft X-ray absorption spectroscopy. Phys Rev B, 2010, 82: 184429
33 Hopkins EJ, Prots Y, Burkhardt U, *et al.* $Ba_3V_2S_4O_3$: a Mott insulating frustrated quasi-one-dimensional $S$=1 magnet. Chem Eur J, 2015, 21: 7938–7943
34 Wong CJ, Hopkins EJ, Prots Y, *et al.* Anionic ordering in $Ba_{15}V_{12}S_{34}O_3$, affording three oxidation states of vanadium and a quasi-one-dimensional magnetic lattice. Chem Mater, 2016, 28: 1621–1624
35 Jin CQ, Zhou JS, Goodenough JB, *et al.* High-pressure synthesis of the cubic perovskite $BaRuO_3$ and evolution of ferromagnetism in $ARuO_3$ (A=Ca, Sr, Ba) ruthenates. Proc Natl Acad Sci USA, 2008, 105: 7115–7119
36 Rhodes P, Wohlfarth EP. The effective curie-weiss constant of ferromagnetic metals and alloys. Proc R Soc Lond A, 1963, 273: 247–258
37 Mao Q, Chen B, Yang J, *et al.* Critical properties of the quasi-two-dimensional metallic ferromagnet $Fe_{2.85}GeTe_2$. J Phys-Condens Matter, 2018, 30: 345802
38 Kurniawan B, Ishikawa M, Kato T, *et al.* Novel three-dimensional magnetic ordering in the quantum spin system $NH_4CuCl_3$. J Phys-Condens Matter, 1999, 11: 9073–9080
39 Hardy V, Lambert S, Lees MR, *et al.* Specific heat and magnetization study on single crystals of the frustrated quasi-one-dimensional oxide $Ca_3Co_2O_6$. Phys Rev B, 2003, 68: 014424
40 Zhang J, Duan L, Wang Z, *et al.* The synthesis of a quasi-one-dimensional iron-based telluride with antiferromagnetic chains and a spin glass state. Inorg Chem, 2020, 59: 5377–5385
41 Zhang J, Liu M, Wang X, *et al.* $Ba_9V_3Se_{15}$: a novel compound with spin chains. J Phys-Condens Matter, 2018, 30: 214001


**Acknowledgements** This work was supported by the National Key R&D Program of China and the National Natural Science Foundation of China (2018YFA0305700, 11974410, 2017YFA0302900, 2015CB921300, 11534016 and 11974062).

**Author contributions** Jin C and Wang X conceived and supervised this project. Duan L preformed most of experiments including the synthesis, characterizations and physical properties measurement with the assistance of Zhang J, Li W, Zhao J, Cao L, Deng Z and Yu R. Hu Z, Lin HJ, and Chen CT performed the XAS measurements and data analysis. The calculations were carried out by Zhan F and Wang R. Duan L, Wang X and Jin C wrote the paper in discussion with other co-authors.

**Conflict of interest** The authors declare that they have no conflict of interest.

**Lei Duan** is currently a PhD candidate at the Institute of Physics, Chinese Academy of Sciences (IOPCAS). He received his BSc degree (majored in physics) from Jilin University, China in 2010. His PhD research focuses on using high-pressure technique to explore and synthesize new quantum materials such as superconductors and quasi one-dimensional (1D) materials.

**Xiancheng Wang** is currently an associate professor at the IOPCAS. He received his PhD degree from Jilin University in 2005, and then became a postdoctoral fellow in Tsinghua University. Since 2008, he has worked at IOPCAS. His research interests include exploring new materials especially using high pressure technique and studying their novel physics, such as superconductors and the materials with quasi one-dimensional (1D) spin chains or 1D conducting chains.

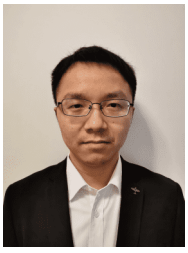

**Rui Wang** received his PhD degree in condensed matter physics from Chongqing University (CQU), China in 2012. He then worked as a faculty in CQU. In 2017–2018, he came to Southern University of Science and Technology as a senior visiting scholar. Currently, he is an associate professor in the Department of Physics, CQU. His research interests include computational condensed matter physics, design of topological insulators and semimetals, and defect physics.

**Changqing Jin** received his PhD degree at the IOPCAS in 1991. He was an associate professor (1996), and is currently a professor (1998) at the IOPCAS. He is team leader of IOPCAS on studies of new emergent materials by design especially *via* developing synergetic high-pressure extreme conditions.

  

# 一种新型铬基砷化物$La_3CrAs_5$的高压合成、结构表征及物性研究

段磊[1,2], 望贤成[1*], 詹方洋[3], 张俊[1,2], 胡志伟[4], 赵建发[1,2], 李文敏[1,2], 曹立朋[1,2], 邓正[1], 于润泽[1], 林宏基[5], Chien-Te. Chen[5], 王锐[3*], 靳常青[1,2,6*]

**摘要** 本文中，我们利用高温高压法，在La-Cr-As体系中发现并成功制备了第一个新的三元化合物材料$La_3CrAs_5$. 该化合物属于六方反$Hf_5Sn_3Cu$型结构, 其空间群为$P_3/mcm$, 晶格参数为$a=b=8.9845$ Å, $c=5.8897$ Å. $La_3CrAs_5$的晶体结构含有沿$c$轴方向的共面连接$CrAs_6$八面体链，这些一维自旋链在$ab$平面内以三角格子形式进行排列，链与链之间的距离为8.9845 Å. 研究表明，$La_3CrAs_5$具有三维金属导电性质，并且在低温条件下遵循费米液行为；另外，$La_3CrAs_5$中$CrAs_6$自旋链由于巡游电子关联, 在50 K发生三维铁磁相变. 理论计算表明，La对费米面附近态密度的贡献是不可忽略的，导致$La_3CrAs_5$成为了一个三维金属. 此外，我们还计算了晶体轨道哈密顿数(−COHP)来解释$La_3CrAs_5$结构的整体稳定性以及化学键特征.

  